Open Access Full Text Article

ORIGINAL RESEARCH

Near-infrared nanoparticles based on indocyanine green-conjugated albumin: a versatile platform for imaging-guided synergistic tumor chemo-phototherapy with temperature-responsive drug release

Yuxin Ma[1]
Xiaohua Liu[1]
Qianli Ma[2]
Yizhi Liu[3]

[1]Jinan Stomatologic Hospital, Jinan 250001, Shandong, China; [2]School and Hospital of Stomatology, Shandong University, Jinan 250001, Shandong, China; [3]Binzhou Medical School, Binzhou 256603, Shandong, China

Background: The aim of this study was to develop a multifunctional theranostic agent based on BSA nanoparticles (NPs), which loaded artemisinin (ART) and co-conjugated with indocyanine green (ICG) and arginine-glycine-aspartic acid (RGD) peptide (RGD-indocyanine green-Bovine Serum Albumin- artemisinin [IBA] NPs).

Materials and methods: The physicochemical parameters of RGD-IBA NPs were characterized in terms of the particle size, zeta potential, morphology, entrapment efficiency, drug loading, in vitro release behavior, photothermal and photodynamic effect, and in vitro anticancer ability. In vivo fluorescence and thermal imaging as well as antitumor studies were also evaluated.

Results: The tumor chemotherapeutic effects of ART and the ability of fluorescence imaging, hyperthermia generation and reactive oxygen species production of ICG and tumor-targeting RGD were integrated to achieve RGD-IBA NPs for imaging-guided tumor-targeted chemotherapy/photothermal/photodynamic therapy (chemo-phototherapy). The RGD-IBA NPs showed enhanced physiological stability and photo-stability compared with free ART and ICG. In addition, they were temperature-responsive; their sizes increased with increasing temperature between 25°C and 55°C, thereby leading to drug release upon the irradiation with near infrared (NIR) laser. In vivo fluorescence images of tumor-bearing mice showed that the RGD-IBA NPs could highly and passively reach the targeted tumor region with maximum accumulation at 24 hours post-intravenous injection. The in vitro and in vivo results demonstrated that the RGD-IBA NPs not only have good biocompatibility, but also are highly efficient tumor synergistic chemo-phototherapeutic agents.

Conclusion: Through this study, it was found that RGD-IBA NPs could potentially be a very promising tumor theranostic agent.

Keywords: artemisinin, indocyanine green, theranostic, imaging-guided tumor therapy, chemo-phototherapy

Introduction

Cancer is a life threatening disease worldwide, and chemotherapy (CHT) is a current major treatment for most cancer due to its high efficiency.[1] However, some shortcomings of CHT in clinical practice have been reported; for example, it easily produces drug resistance, systemic toxicity and tumor recurrence.[2–4] Consequently, there is an urgent need to develop chemotherapeutic agent carriers that can achieve simultaneous drug loading, targeted delivery and controlled release to obtain maximum therapeutic effect

Correspondence: Xiaohua Liu
Jinan Stomatologic Hospital, Jinan 250001, Shandong, China
Tel +86 531 8666 6920
Email liuxhmed@foxmail.com

with minimal side effects to normal tissue.[5–10] Phototherapy (PT) such as combined photothermal therapy and photodynamic therapy (PTT-PDT) is an emerging highly compatible therapeutic modality.[11] This method uses light to trigger agents, which then cause the generation of hyperthermia or the production of reactive oxygen species (ROS) that can kill tumor cells.[12,13] Since PTT-PDT is an emerging non-invasive tumor therapeutic strategy, it has attracted increasing attention. Although PTT-PDT is accompanied by a number of side effects, which, however, are fewer than conventional treatments, it has been reported to have a potential risk like tumor relapse.[14] The combination of CHT and PTT-PDT, which has synergistic effects, has been reported to have a relatively better tumor therapeutic effect.[15,16] In addition, the release of drug on some PTT-PDT agents could be triggered by light irradiation. This may prolong drug action time, and therefore enhance the therapeutic effect.[17,18]

Currently, endowing the chemo-phototherapeutic agent with imaging function for diagnostic purpose can allow real-time monitoring of the behavior of agents in vitro and in vivo and thus can lead to guided cancer therapy.[19,20] Indocyanine green (ICG) is an amphiphilic dye that has been approved by the US Food and Drug Administration for near infrared (NIR) clinical fluorescence imaging.[21,22] Since it has high molar extinction coefficient at 780-nm wavelength, it possesses high NIR photothermal conversion abilities. In addition, ICG has been reported to generate ROS when irradiated with NIR laser, leading to cell apoptosis.[23,24] Therefore, ICG has been regarded as the most suitable theranostic agent that has combined imaging and PPT-PDT functions. Nevertheless, the application of free ICG is restricted by its limitations, such as high aggregation ability in aqueous solutions with concentration-dependent manner, poor photo-stability, lack of specificity and quick body clearance ($t_{1/2} \approx$ 2–4 minutes).[25–27]

Artemisinin (ART) is a natural anti-malaria drug.[28,29] In recent years, it has been reported to have potential anti-cancer activities against several cancer types, such as liver cancer, breast cancer and lung cancer.[30–32] Compared with traditional anticancer drugs (eg, DOX and PTX), ART exhibits lower side effects as well as risk of recurrence and metastasis. However, ART is nearly insoluble, and therefore cannot easily achieve local treatment. To overcome these drawbacks, delivery of ICG and ART through carriers such as nano-graphene oxide, polymers, transition metal dichalcogenides and protein has been reported to be a better therapeutic strategy.[33] Among these carriers, protein is regarded as a potential drug carrier due to its high biocompat-ibility and modifiable surface chemistry, which is safe for in vivo application.[34]

In this work, a multifunctional theranostic agent was designed and prepared based on BSA nanoparticle (NP), which loaded ART. This agent was further covalently conjugated with ICG and tumor-specific moiety, arginine-glycine-aspartic acid (RGD)-peptide, for imaging-guided chemo-phototherapy (Figure 1). The prepared RGD-indocyanine green-Bovine Serum Albumin- artemisinin (IBA)NPs have great biocompatibility, water stability, photo-stability and photothermal effect. Upon NIR laser irradiation, the RGD-IBA NPs could simultaneously generate hyperthermia and ROS, and thereby trigger drug release and destroy tumor cells. The monitoring through in vivo fluorescence imaging showed that the RGD-IBA NPs could target tumor and accumulate in tumor region at 24 hours post-intravenous injection. The in vitro and in vivo results demonstrated that the RGD-IBA NPs had synergistic anticancer efficacy.

Materials and methods
Materials
ART (purified ≥98.0%) was obtained from Shanghai Ryon Biological Technology Co., Ltd, Shanghai, China. 1-ethyl-3-(3-dimethylaminopropyl) carbodiimide (EDC), N-hydroxysuccinimide (NHS), ICG and BSA (purified ≥98.0%) were purchased from Sigma-Aldrich (Co., St Louis, MO, USA). NH_2-$PEG_{2,000}$-RGD was purchased from Shaanxi BEO Biotechnology co., Ltd (Xi'an, China). Sulfo ICG-NHS ester was obtained from Xi'an Ruixi Biotechnology co., Ltd (Xi'an, China). RPMI 1640 cell media, FBS and PBS were obtained from Invitrogen (Carlsbad, CA, USA). Cell counting kit-8 (CCK-8) was supplied by Dojindo Laboratories (Kumamoto, Japan).

Synthesis and characterization of RGD-IBA NPs
To incorporate ART into the BSA NPs, the self-assembly method with a little modification was adopted. In detail, 15 mg ART was dissolved in DMSO and dispersed into 10 mL BSA solution (1 mg/mL, dissolved in distilled water) with magnetic stirring for 6 hours at 37°C. In total, 300 µL 0.5% glutaraldehyde was then used for cross-linking. After that, the mixture was dialyzed against distilled water (MW cut off =12 kDa) for 1 day to purify BSA-ART solution. Next, sulfo ICG-NHS ester (3 mg) was added into the BSA-ART solution and stirred for 2 hours to result in ICG-BSA-ART solution. Then, NH_2-$PEG_{2,000}$-RGD (3 mg) was dispersed into the ICG-BSA-ART solution under the presence of 10 µL
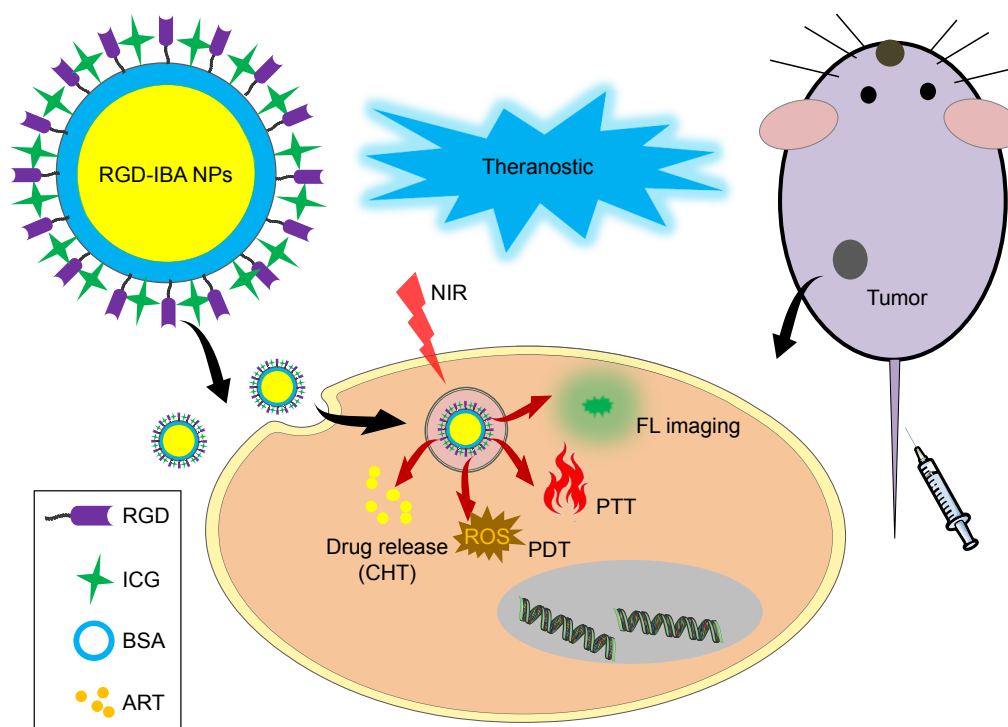
Figure 1 Synthesis and application schematic.
Note: The schematic of the RGD-IBA NPs, which were applied for tumor theranostics combined with chemotherapy, PTT and PDT.
Abbreviations: ART, artemisinin; BSA, bovine serum albumin; CHT, chemotherapy; FL, fluorescence; ICG, indocyanine green; NIR, near infrared; NPs, nanoparticles; PDT, photodynamic therapy; PTT, photothermal therapy; RGD, arginine-glycine-aspartic acid; IBA, indocyanine green-Bovine Serum Albumin- artemisinin.

EDC (5 mg/mL) and 15 μL NHS (20 mg/mL). The mixture was reacted for 2 hours at 4°C with slight stirring, and purified by dialysis against distilled water (MW cut off =12 kDa) for 1 day, resulting in RGD-ICG-BSA-ART NPs (RGD-IBA NPs). The morphology, size and zeta potential of the NPs were observed and detected by a transmission electron microscope (TEM, JEM-100S; JEOL, Tokyo, Japan) and a dynamic light scattering (DLS) method (BI-9000AT, Brookhaven, Holtsville, NY, USA), respectively. The amount of loaded ART and ICG was detected by UV-vis spectrophotometer (UV3100, Shimadzu, Kyoto, Japan) by monitoring the absorption peak at 290 nm and 780 nm, respectively, according to the following equation:

$$\text{Loading ratio (\%)} = \frac{M_{\text{initial drug}} - M_{\text{drug in dialyzate}}}{M_{\text{nanoparticles}}}$$

Cell culture

The human oral epidermal carcinoma KB cells were purchased from Shanghai Institute of Cell Biology (Shanghai, China) and were incubated in RPMI 1640 medium (11875; Thermo Fisher Scientific, Waltham, MA, USA) supplemented

with 10% FBS in a humidified atmosphere containing 5% CO_2 at 37°C.

Photothermal performance of RGD-IBA NPs

The photothermal effect of RGD-IBA NPs was evaluated by detecting the temperature variation of RGD-IBA NPs dispersion (0.75 mL) under irradiation of 808 nm laser for 5 minutes with a power intensity of 1 W/cm². As control, the temperature of the PBS, free ICG, RGD-IB NPs with the same ICG concentration was recorded by an infrared thermal imaging camera (Ti27; Fluke Corporation, Everett, WA, USA).

In vitro ROS detection

To detect intracellular ROS level for evaluating PDT effect, the KB cell lines were treated by H_2O_2, NIR irradiation, ICG+ NIR, RGD-IBA NPs and RGD-IBA NPs + NIR and stained with the fluorescent dye, 2′,7′- dichlorofluorescein diacetate (DCFH-DA). The cells treated by 200 μL H_2O_2 (50 mM) at 37°C for 30 minutes were set as positive control. DCFH-DA was first dissolved in DMSO (10 mM) and then was incubated with the treated cells for 1 hour at 37°C. Next, the stained cells were washed by PBS three times and

irradiated under the 808 nm laser (1 W/cm^2) for 5 minutes. A commercial confocal laser scanning microscopy (Zeiss LSM 700, Oberkochen, Germany) was used to detect ROS (Ex =488 nm, Em =515–540 nm). In addition, a flow cytometer (Becton Dickinson, San José, CA, USA) was used to quantitatively measure the intracellular ROS generation.

In vitro cytotoxicity

A classic CCK-8 assay was used to investigate the in vitro cytotoxicity. In detail, 1×10^4 KB cells in 100 µL of medium were seeded into 96-well plates and incubated for 24 hours. The cells were then treated with PBS, free ICG, free ART, IBA NPs or RGD-IBA NPs at concentrations of 0, 10, 20, 30, 40 or 50 µg/mL ART for 5 hours. The cells were treated with or without laser irradiation by 808 nm laser at 1.0 W/cm^2 for 5 minutes. The temperature of the irradiated cells was recorded by an infrared thermal imaging camera. After irradiation, the cells were cultured at 37°C for 24 hours. After that, the cell viability was measured by the CCK-8 assay and the absorbance value of the cells at 450 nm was detected by a microplate reader (EnVision; PerkinElmer, Waltham, MA, USA).

Animals and tumor model

Female balb/c mice (4–6 weeks old) were obtained from Charles River Laboratories (Beijing, China). The animals' experiments were conducted in accordance with the Guidance Suggestions for the Care and Use of Laboratory Animals. The procedures were approved by Animal Care and Use Committee of Binzhou Medical University. To establish the KB tumor model, 2×10^6 KB cells were subcutaneously injected into the flank region of the mice. Tumor volume was calculated as length × width^2/2.

In vivo NIR fluorescence imaging

When the tumor volume reached 100 mm^3, free ICG, IBA NPs and RGD-IBA NPs (10 mg/kg) were intravenously injected into the tumor-bearing mice, and imaged by a Maestro in vivo fluorescence imaging system (CRi Inc., Woburn, MA, USA) with a 704 nm excitation wavelength and 745 nm filter. The mice were anesthetized with isoflurane and were imaged at 0, 0.1, 12, 24 and 36 hours post-injection.

In vivo tumor chemo-phototherapy

When the tumors had grown to about 100 mm^3, the tumor-bearing mice were randomly divided into six groups (n=5) and then were intravenously administered with saline, ART, IBA NPs and RGD-IBA NPs with or without NIR, respectively. After 24 hours of injection, the tumors of mice were irradiated by the 808 nm laser (1.0 W/cm^2) for 5 minutes.

The temperature changes of the tumor regions during laser irradiation were monitored by the infrared thermal imaging camera. The tumor volume and body weight of each mouse in these treated groups were recorded every 3 days for a total of 27 days.

In vivo toxicity evaluation

To investigate the toxicity of RGD-IBA NPs in vivo, ten healthy mice were divided into two groups and intravenously injected with saline and RGD-IBA NPs (15 mg/kg), respectively. One month after injection, major organs including heart, liver, spleen, lung and kidney from each mouse were harvested, fixed in formalin, processed routinely into paraffin, sectioned, stained with hematoxylin and eosin (HE) and examined by a digital microscope. Moreover, the whole blood of the treated mice was collected for blood analysis at 0, first and 30th day post-injection. The complete blood counts were measured in Jinan Stomatologic Hospital.
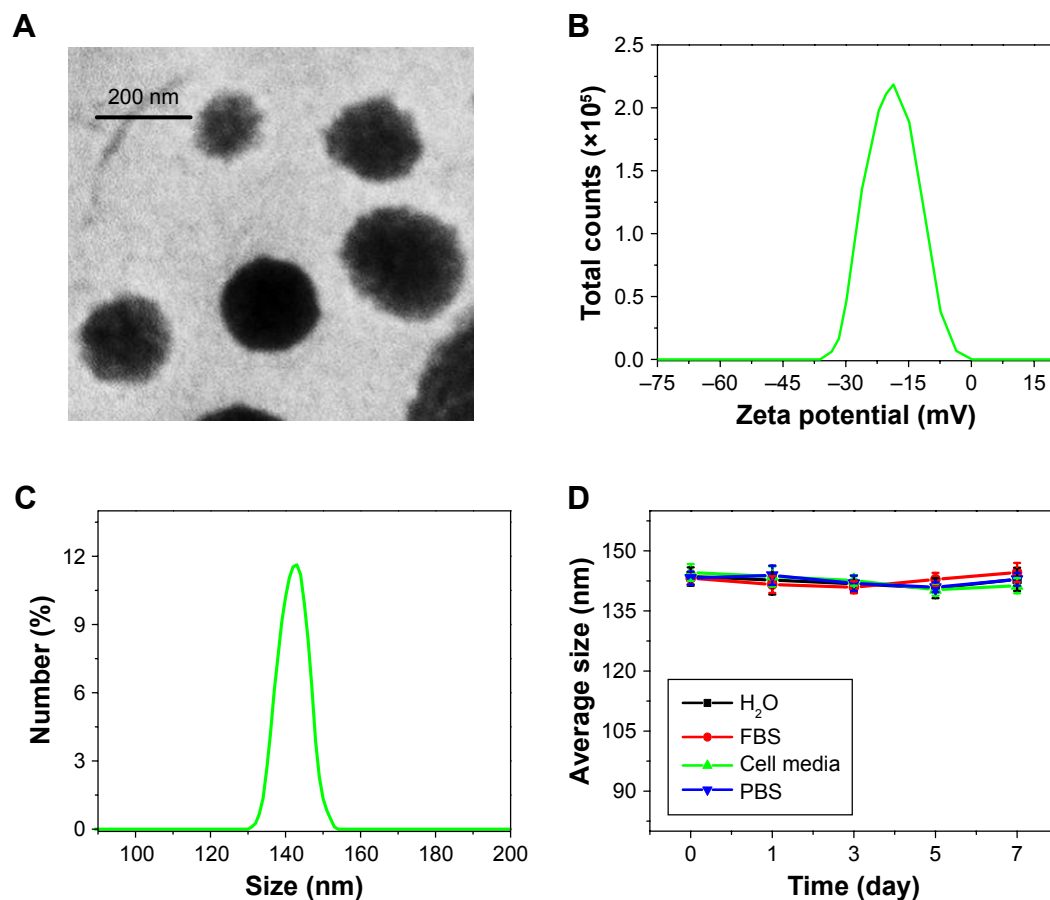
Statistical analysis

Data were shown as mean ± SD. Two-tailed Student's t-test was used to analyze the statistical significance of two groups. The differences were considered significant for *$P<0.05$ and highly significant for **$P<0.01$.

Results and discussion
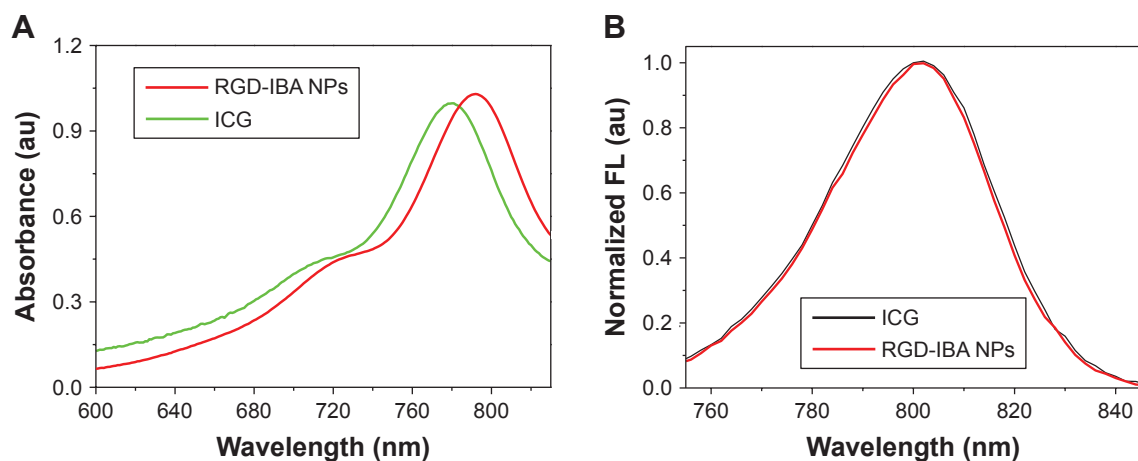## Preparation and characterization of RGD-IBA NPs

As shown Figure 2A, the TEM image showed that the RGD-IBA NPs were uniformly spheres. The DLS analysis demonstrated that the surface potential and average diameter of RGD-IBA NPs were −20.51 mV and 141.54 nm, respectively (Figure 2B and C). Furthermore, the average sizes of RGD-IBA NPs in water, FBS, cell media and PBS showed no considerable changes over a period of 1 week (Figure 2D), demonstrating that RGD-IBA NPs have high physiological stability, most likely due to PEG and BSA encapsulation.[35,36] The calculation showed that ART and ICG encapsulation efficiencies were calculated to be about 89.56%±2.19% and 71.85%±1.52%, respectively.

The absorption spectra of free ICG and RGD-IBA NPs with the same ICG concentration are shown in Figure 3A. The absorbance peak of RGD-IBA NPs was red-shifted by 18 nm from 780 nm to 798 nm, likely due to some self-aggregation of ICG molecules on the surface of NPs.[22] In addition, Figure 3B shows that the fluorescence spectrum of RGD-IBA NPs is similar to that of free ICG, indicating that RGD-IBA NPs have fluorescence imaging capability, which is similar to the capacity of ICG.

Figure 2 Morphology and stability characterization.
Notes: The (**A**) TEM image, (**B**) zeta potential and (**C**) size distribution of RGD-IBA NPs. (**D**) The average size change of RGD-IBA NPs in water, FBS, cell media and PBS for 7 days.
Abbreviations: NPs, nanoparticles; RGD, arginine-glycine-aspartic acid; TEM, transmission electron microscopy.

For photothermal performance, the NPs were irradiated with 808 nm laser (1.0 W/cm^2) for 5 minutes. The temperature of PBS (control) was slightly increased. By contrast, the temperature of RGD-IBA NPs as well as of RGD-IB NPs (without ART) was rapidly increased, reaching a peak temperature of 33.9°C, which is higher than the temperature of free ICG (24.1°C) (Figure 4A and B). This is likely due to the enhanced ICG stability and the higher
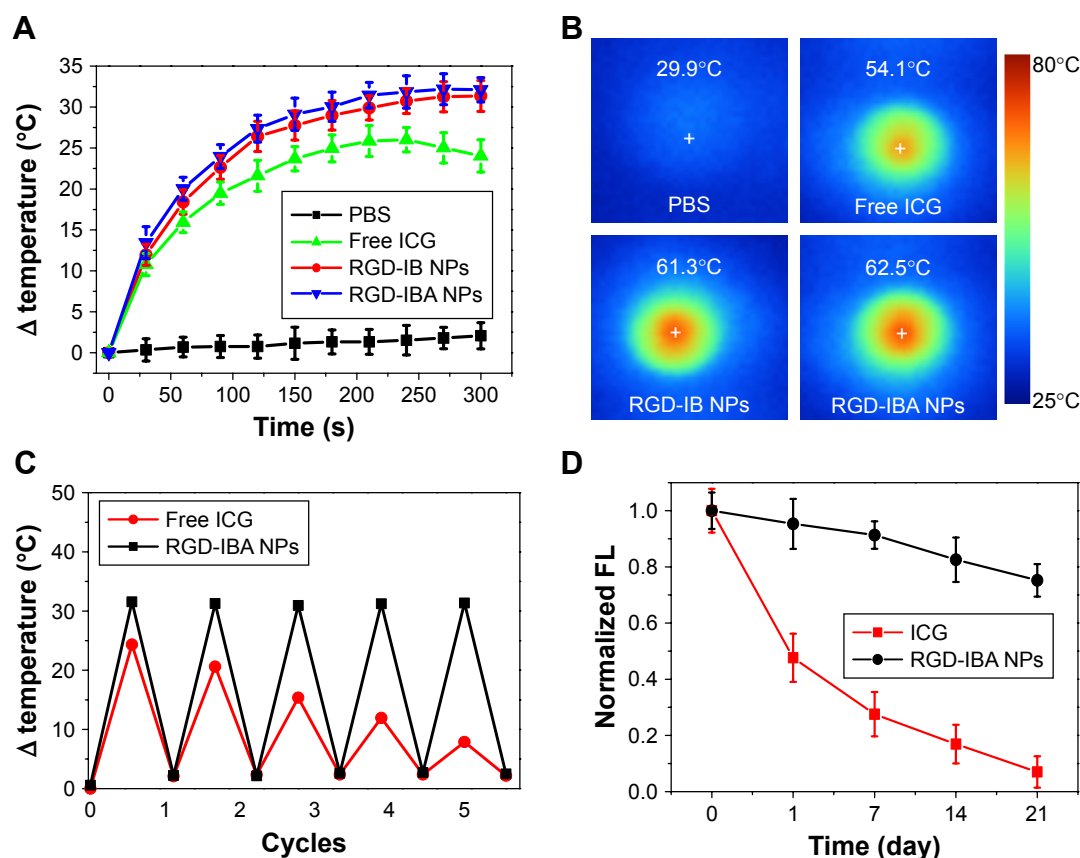

Figure 3 Spectra characterization.
Note: (**A**) The absorbance and (**B**) fluorescence spectra of free ICG and RGD-IBA NPs with the same ICG concentration.
Abbreviations: ART, artemisinin; FL, fluorescence; ICG, indocyanine green; NPs, nanoparticles; RGD, arginine-glycine-aspartic acid.

Figure 4 Photothermal effect and thermal stability.

Notes: (**A**) The temperature change profiles and (**B**) thermal images of PBS, free ICG, RGD-IB NPs and RGD-IBA NPs under the irradiation by 808 nm laser (1.0 W/cm²) for 5 minutes. (**C**) Temperature change of free ICG and RGD-IBA NPs over five cycles of repeated laser irradiation. (**D**) The fluorescence intensity change of free ICG and RGD-IBA NPs in aqueous solution for 21 days.

Abbreviations: ART, artemisinin; FL, fluorescence; ICG, indocyanine green; PTT, photothermal therapy; NPs, nanoparticles; RGD, arginine-glycine-aspartic acid.

absorption of RGD-IBA NPs compared with that of free ICG at 808 nm.

Figure 4C shows the photothermal stability of RGD-IBA NPs after five cycles of NIR irradiation. After five cycles of NIR irradiation, the photothermal stability of RGD-IBA NPs was unchanged, whereas that of free ICG decreased, as indicated by the decrease of temperature over the five cycles. This demonstrates that the RGD-IBA NPs have higher photostability than free ICG, and the photo-stability of free ICG was enhanced when conjugated with BSA NPs. Figure 4D shows the fluorescence stability of free ICG and RGD-IBA NPs. After 21 days of storage, the fluorescence intensity of free ICG decreased to 3.9% of its original fluorescence intensity value, while that of RGD-IBA NPs was 75.2% of its initial value. It is apparent that the fluorescence stability of free ICG was improved after being conjugated with PEG-BSA.

Temperature-responsive drug release

The releases of ART and ICG in RGD-IBA NPs were evaluated. At pH 7.4, the accumulated release ratios of ART and ICG after 36 hours were 23.5% and 11.1%, respectively.

Under 5 minutes of NIR irradiation (808 nm, 1 W/cm²), sudden release of ART, reaching the accumulated release ratio of 61.5%, was observed after six cycles of NIR irradiation. At the same condition, ICG had the accumulated release ratio of only 18.4% (Figure 5A). These results indicate that NIR irradiation-induced local hyperthermia can trigger (with ON/OFF mode) the release of ART from RGD-IBA NPs. The release of ICG was hardly temperature sensitive, likely due to the covalent conjugation between ICG and RGD-IBA NPs, which is stronger than non-covalent conjugation.[37] To furthermore investigate the mechanism of temperature-responsive drug release, RGD-IBA NPs were treated with different temperatures ranging from 25°C to 55°C for 5 minutes. The results showed that the diameter of RGD-IBA NPs was increased from 35°C to 55°C (Figure 5B). This indicates that the temperature-responsive drug release could be through heat-induced expansion of BSA NPs.

ROS production of RGD-IBA NPs

ROS has high cytotoxicity and can kill cancer cells. To investigate the NIR irradiation-induced ROS generation, KB cells
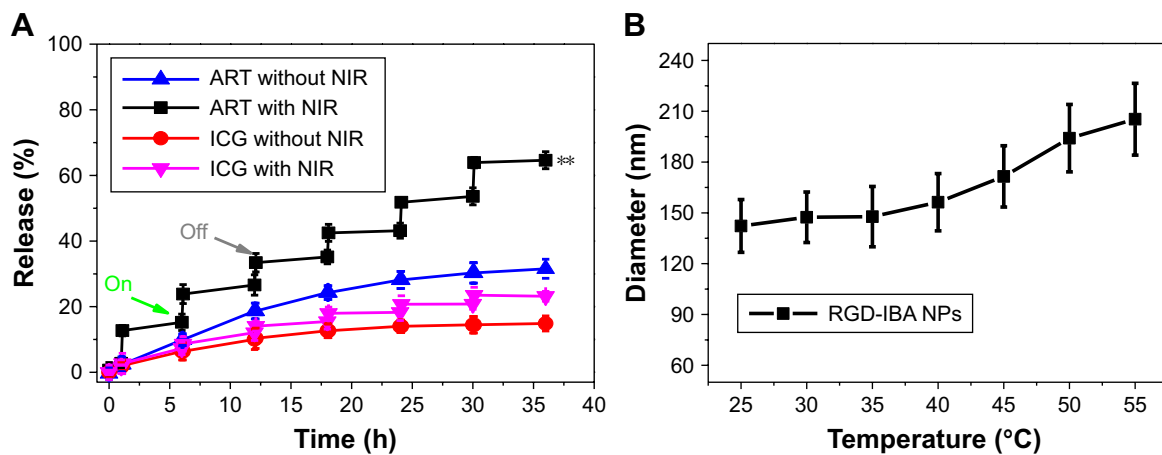
Figure 5 Drug release.
Notes: (**A**) Release kinetics of ART or ICG from RGD-IBA NPs in PBS buffer (pH =7.4) with or without NIR laser irradiation. The ART with NIR group compared with other groups, **$P<0.01$. (**B**) The diameter change of RGD-IBA NPs under the various temperature treatments.
Abbreviations: ART, artemisinin; ICG, indocyanine green; NIR, near infrared; NPs, nanoparticles; RGD, arginine-glycine-aspartic acid.

were incubated with H_2O_2 (as a positive control), free ICG and RGD-IBA NPs (with the same ICG concentration), with or without 5 minutes of NIR irradiation (1 W/cm^2). As shown in Figure 6A, after being stained by DCFH-DA, high intensity of green fluorescence signal was detected in RGD-IBA NPs + NIR-treated cells and H_2O_2-treated group, indicating that RGD-IBA NPs + NIR could sufficiently generate ROS. Conversely, free ICG + NIR-treated group exhibited negligible intensity of green fluorescence signal, similarly to the negative control, suggesting that the cellular uptake of free ICG is low. Similar conclusions can be seen in Figure 6A, and the statistical results achieved by flow

cytometry are shown in Figure 6B. Thus, this suggests that NIR can trigger RGD-IBA NPs to abundantly produce ROS, which is beneficial for tumor PDT.

In vitro synergistic tumor chemo-phototherapy

Figure 7A shows the temperature change of KB cells treated with PBS, ICG, IBA NPs and RGD-IBA NP solutions (with the same ICG concentration) under NIR irradiation for 5 minutes (1.0 W/cm^2). The results indicated that cells treated with RGD-IBA NPs had the largest temperature increase ($\Delta T=23°C$) compared to cells treated with ICG, IBA NPs
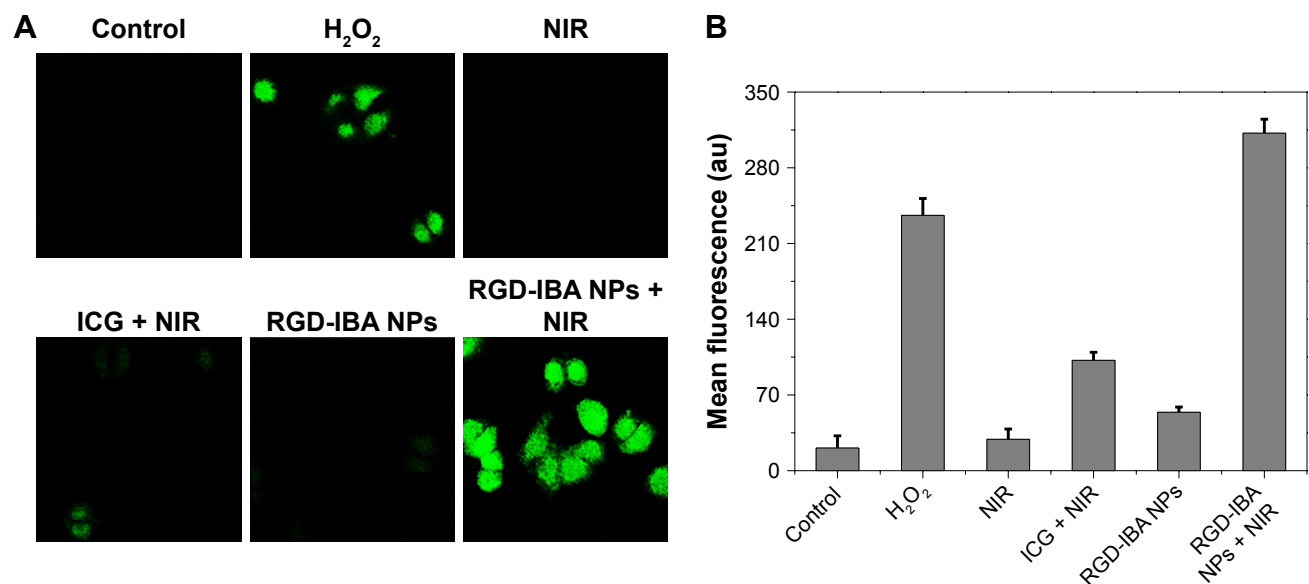

Figure 6 In vitro ROS detection.
Notes: (**A**) The fluorescence images of KB cells after different treatments as indicated. Green was the fluorescence signal of ROS indicator DCFH-DA. Scale bar =60 μm.
(**B**) Quantification of induced ROS intensity achieved by flow cytometry.
Abbreviations: ART, artemisinin; DCFH-DA, dichlorofluorescein diacetate; ICG, indocyanine green; NIR, near infrared; NPs, nanoparticles; RGD, arginine-glycine-aspartic acid; ROS, reactive oxygen species.
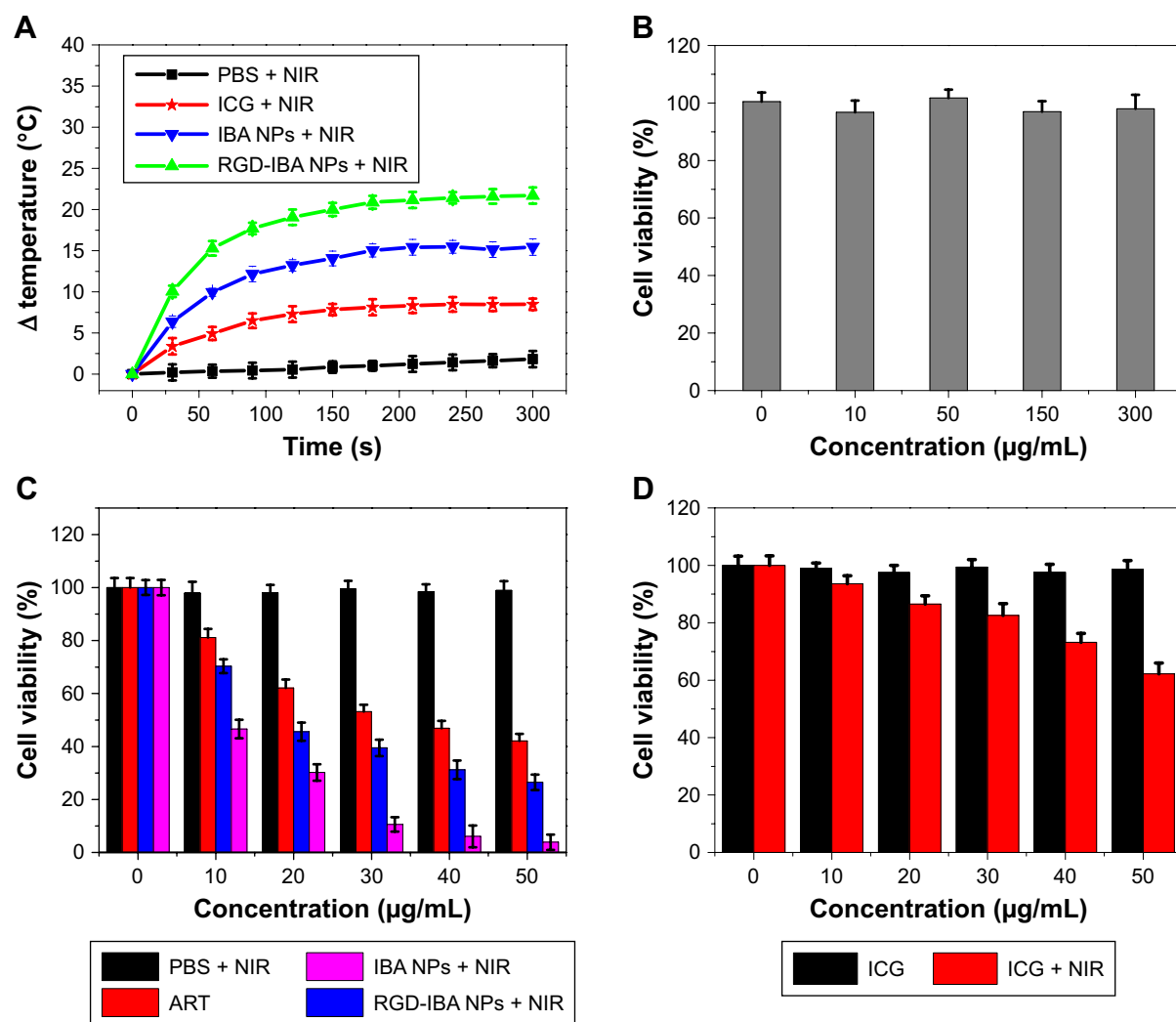
Figure 7 In vitro cytotoxicity.

Notes: (**A**) The temperature change curves of PBS, free ICG, IBA NPs and RGD-IBA NPs under NIR irradiation with an 808 nm laser for 5 minutes. (**B**) Cell viability of KB cells treated with different concentration of RGD-IB NPs. (**C**) Cell viability of KB cells treated with PBS, IBA NPs, ART and RGD-IB NPs (at the same concentration of ART) under NIR irradiation for 5 minutes ($1.0 \, W/cm^2$). (**D**) Cell viability of KB cells treated with free ICG with or without 5 minutes NIR irradiation ($1.0 \, W/cm^2$).

Abbreviations: ART, artemisinin; ICG, indocyanine green; NIR, near infrared; NPs, nanoparticles; PTT, photothermal therapy; RGD, arginine-glycine-aspartic acid.

and PBS due to enhanced internalization effect of RGD-IBA NPs mediated by RGD-targeted effect.

Classical CCK-8 assay was used to evaluate in vitro cytotoxicity of the PT. Without laser irradiation, RGD-IB NPs (RGD-IBA NPs without ART) had no cytotoxicity, indicating that they, the carriers of ART, have good biocompatibility (Figure 7B). On the other hand, with laser irradiation, the viability of KB cells incubated with RGD-IBA NPs was significantly decreased with increasing RGD-IBA NP concentration. Nearly 96.5% of cells incubated with 50 µg/mL RGD-IBA NPs were dead, which is the highest among that of cells incubated with free ART, PBS + NIR and IBA NPs + NIR (Figure 7C). As controls, ICG and ICG + NIR had low effects on cell viability (Figure 7D).

Although free ICG has been reported to produce ROS and kill cells, its cellular uptake is low. It appears that the effects of RGD-IBA NPs triggered with NIR irradiation on cell viability are high because of the synergistic effects.

In vivo NIR fluorescence and thermal imaging

As shown in Figure 8A, at 0.1 hour post-intravenous injections of free ICG, IBA NPs and RGD-IBA NPs, strong fluorescence signal was observed throughout the body of mice. However, at 24 hours post-intravenous injection, stronger fluorescence signal was observed only in the tumor region of RGD-IBA NPs-treated mice. According to the corresponding statistical results (Figure 8B), the fluorescence signal intensity in the
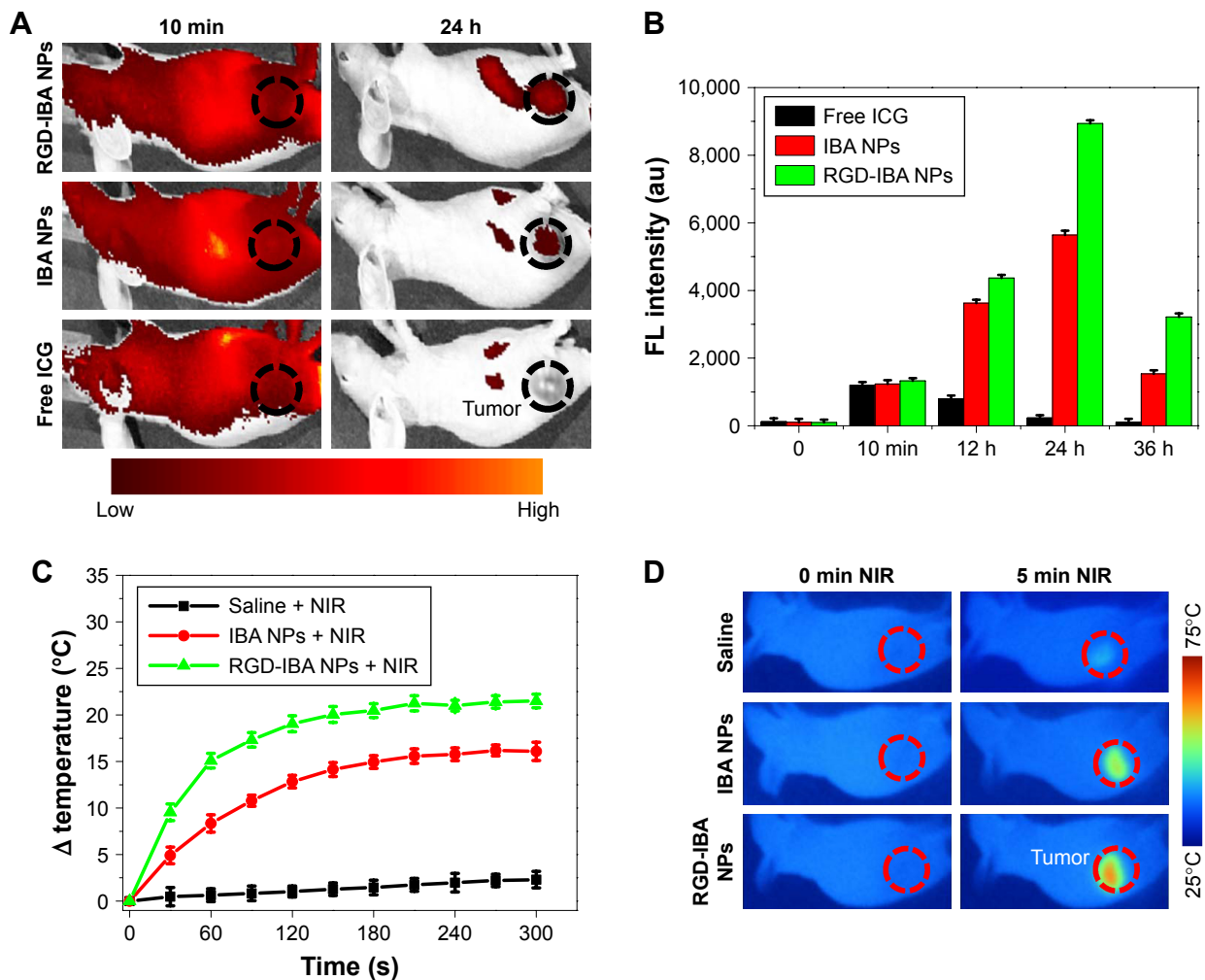
Figure 8 In vivo NIR fluorescence and thermal imaging.

Notes: (**A**) Fluorescence signal was obtained in tumor sites at 10 minutes and 24 hours after intravenous administration of free ICG, IBA NPs and RGD-IBA NPs. (**B**) The quantitative analysis of fluorescence intensity in tumor sites at 0 minute, 10 minutes, 12 hours, 24 hours and 36 hours after intravenous administration of free ICG, IBA NPs and RGD-IBA NPs. (**C**) The tumor temperature change of tumor-bearing mice after 24 hours of intravenous injection of saline, IBA NPs and RGD-IBA NPs and durations NIR irradiation (808 nm, 1 W/cm²). (**D**) The corresponding thermal images of tumor-bearing mice before and after 5 minutes of irradiation.

Abbreviations: ART, artemisinin; FL, fluorescence; ICG, indocyanine green; NIR, near infrared; NPs, nanoparticles; RGD, arginine-glycine-aspartic acid.

tumor of RGD-IBA NPs-treated group gradually increased and reached the maximum value at 24 hours after injection; the maximum value is the highest among the fluorescence signal in tumor of free ICG- and IBA NPs-treated groups. The high accumulation of RGD-IBA NPs in tumor is due to the RGD, which can facilitate the binding of NP to its specific target, $\alpha_v\beta_3$ integrin receptor, on tumor tissue.[38]

Based on the fluorescence images, at 24 hours post-intravenous injections of saline, IBA NPs and RGD-IBA NPs, the temperature of tumor regions of mice receiving 808 nm laser irradiation (1 W/cm²) for 5 minutes was recorded using a thermal imager. As shown in Figure 8C and D, the tumor temperature of RGD-IBA NPs-treated group was increased to 20.2°C, which is the highest among all treated groups. This result further demonstrates that RGD-IBA NPs can

largely accumulate in tumor cells, thereby producing high and efficient photothermal effects that can be used in tumor PTT-PDT in vivo.

In vivo synergistic tumor chemo-phototherapy

To assess the synergistic therapeutic effect of combined RGD-IBA NPs and CHT/PTT/PDT, the KB tumor-bearing mice were divided into six groups. As shown in Figure 9A, the saline- and saline + NIR-treated groups showed uninhibited tumor growths. By contrast, ART- and RGD-IBA NP-treated groups exhibited low tumor growth with some tumor suppression. With NIR irradiation at 24 hours post-injection, RGD-IBA NP-treated group exhibited significant therapeutic effect on the ablation of solid tumor, showing
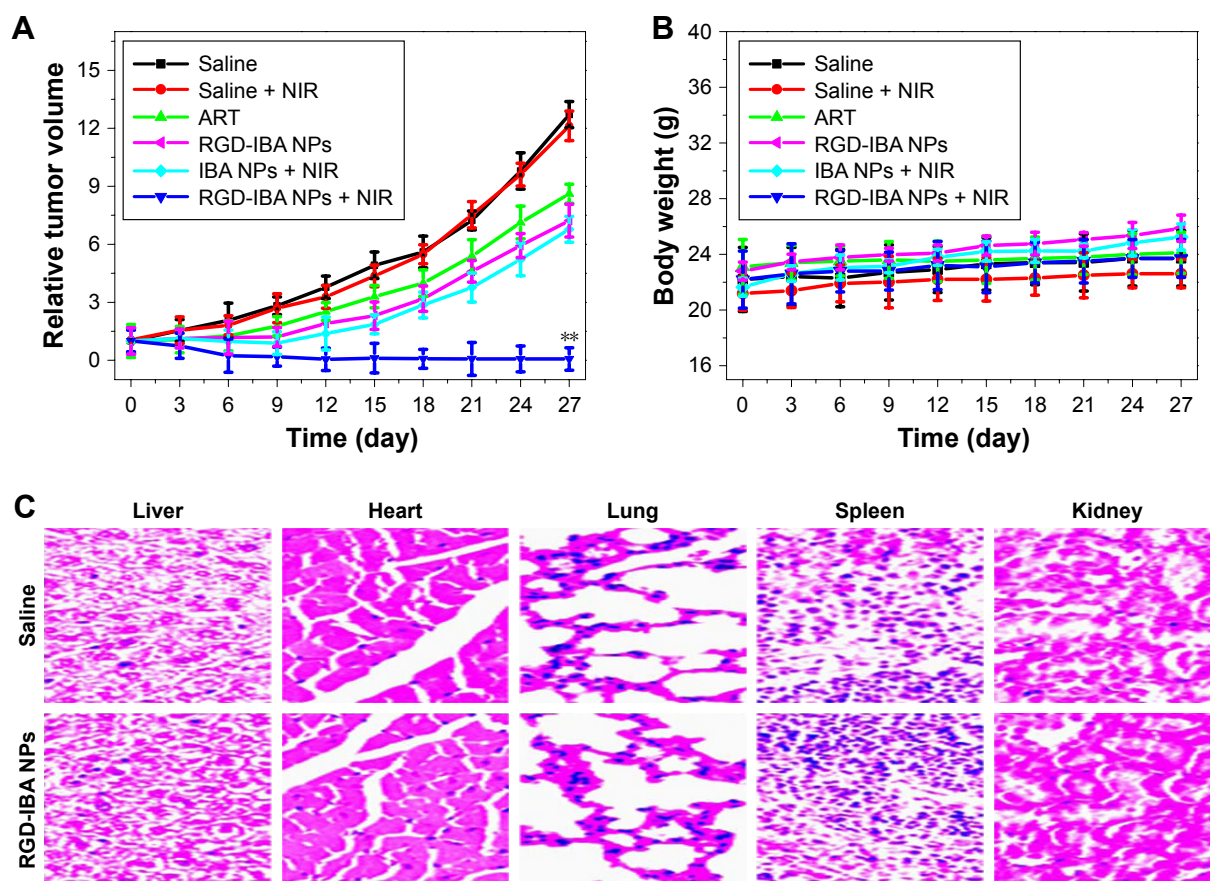
Figure 9 In vivo anticancer.
Notes: (A) The tumor growth profile and (B) body weight of KB tumor-bearing mice after intravenous injection of saline, ART, IBA NPs and RGD-IBA NPs with or without 5 minutes of NIR irradiation (808 nm, 1 W/cm²). The RGD-IBA NPs + NIR group compared with other groups, **$P<0.01$. (C) HE-stained tissue sections of major organs, including the heart, liver, spleen, lung and kidney from mice treated with saline (control) or RGD-IBA NPs at day 30 (magnification: 100×).
Abbreviations: ART, artemisinin; HE, hematoxylin and eosin; ICG, indocyanine green; NIR, near infrared; NPs, nanoparticles; RGD, arginine-glycine-aspartic acid.

complete disappearance of tumor after 27 days of treatment. The body weight losses recorded throughout the treatment period of mice in these groups were not obvious (Figure 9B), implying that the NPs have no obvious acute toxicity. This is likely due to the combined effects of CHT/PTT/PDT, high tumor target effect of RGD-IBA NPs and NIR irradiation-induced ART release, which lead to ROS production and cause hyperthermia. These results demonstrate that the synergistic effects of CHT/PTT/PDT based on RGD-IBA NPs can lead to higher suppression of tumor growth.

In vivo toxicity study

For long-term in vivo toxicity study, RGD-IBA NPs (10 mg/kg) or an equal volume of saline (control) was intravenously injected into healthy Balb/c mice (n=5). After 30 days, major organs including lung, heart, liver, spleen and kidney were harvested and stained with HE dyes. The HE staining images (Figure 9C) showed that there was no noticeable

organ damage. Meanwhile, whole blood samples of mice were collected at 0, 1 and 30 days for complete blood counts. As shown in Figure 10, the results obtained from 1 day or 30 days post-injection were not significantly different from those from day 0. This demonstrates that RGD-IBA NPs have excellent biocompatibility in vivo.

Conclusion

In summary, we prepared multifunctional theranostic agent, RGD-IBA NPs, for imaging-guided synergistic tumor chemo-phototherapy. The use of NIR irradiation could facilitate RGD-IBA NPs by simultaneous generation of hyperthermia, production of ROS and triggering of anticancer drug release. The stabilities of ART and ICG in aqueous solution were remarkably improved by conjugation with BSA NPs. With the fluorescence properties of ICG, the behavior of RGD-IBA NPs could be monitored by in vivo imaging system in guided tumor therapy. The in vitro and in vivo results demonstrated
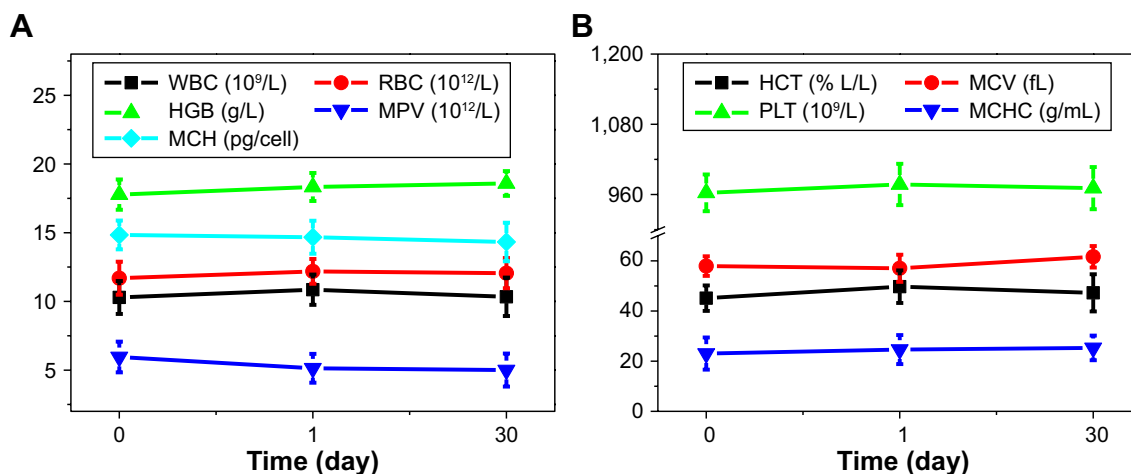
Figure 10 In vivo biocompatibility.
Notes: (**A**, **B**) The complete blood counts of mice at days 0, 1 and 30 post-injection with RGD-IBA NPs. The complete blood counts, including WBC, RBC, HGB, MPV, MCH, HCT, MCV, PLT, MCHC.
Abbreviations: HCT, hematocrit; HGB, hemoglobin; MCH, mean corpuscular volume; MCHC, mean corpuscular hemoglobin concentration; MCV, mean corpuscular volume; MPV, mean platelet volume; PLT, platelets; RBC, red blood cell; WBC, white blood cell.

that combined CHT/PTT/PDT based on RGD-IBA NPs had synergistic antitumor effect. Additionally, RGD-IBA NPs had no obvious cytotoxicity both in vitro and in vivo. These observations indicate that RGD-IBA NPs can be novel promising materials for molecular imaging-guided tumor chemo-phototherapy.

Acknowledgment

Disclosure

The authors report no conflicts of interest in this work.

References

1. Miller KD, Siegel RL, Lin CC, et al. Cancer treatment and survivorship statistics, 2016. *CA Cancer J Clin*. 2016;66(4):271–289.
2. He Q, Shi J. MSN anti-cancer nanomedicines: chemotherapy enhancement, overcoming of drug resistance, and metastasis inhibition. *Adv Mater*. 2014;26(3):391–411.
3. Tian F, Dahmani FZ, Qiao J, et al. A targeted nanoplatform co-delivering chemotherapeutic and antiangiogenic drugs as a tool to reverse multidrug resistance in breast cancer. *Acta Biomater*. 2018;75:398–412.
4. Zhang W, Shen J, Su H, et al. Co-delivery of cisplatin prodrug and chlorin e6 by mesoporous silica nanoparticles for chemo-photodynamic combination therapy to combat drug resistance. *ACS Appl Mater Interfaces*. 2016;8(21):13332–13340.
5. Kamaly N, Yameen B, Wu J, Farokhzad OC. Degradable controlled-release polymers and polymeric nanoparticles: mechanisms of controlling drug release. *Chem Rev*. 2016;116(4):2602–2663.
6. Pérez-Herrero E, Fernández-Medarde A. Advanced targeted therapies in cancer: Drug nanocarriers, the future of chemotherapy. *Eur J Pharm Biopharm*. 2015;93:52–79.
7. Ramasamy T, Haidar ZS, Tran TH, et al. Layer-by-layer assembly of liposomal nanoparticles with PEGylated polyelectrolytes enhances systemic delivery of multiple anticancer drugs. *Acta Biomater*. 2014; 10(12):5116–5127.

8. Ramasamy T, Ruttala HB, Gupta B, et al. Smart chemistry-based nano-sized drug delivery systems for systemic applications: A comprehensive review. *J Control Release*. 2017;258:226–253.
9. Ramasamy T, Ruttala HB, Chitrapriya N, et al. Engineering of cell microenvironment-responsive polypeptide nanovehicle co-encapsulating a synergistic combination of small molecules for effective chemotherapy in solid tumors. *Acta Biomater*. 2017;48: 131–143.
10. Sundaramoorthy P, Ramasamy T, Mishra SK, et al. Engineering of caveolae-specific self-micellizing anticancer lipid nanoparticles to enhance the chemotherapeutic efficacy of oxaliplatin in colorectal cancer cells. *Acta Biomater*. 2016;42:220–231.
11. Ramasamy T, Ruttala HB, Sundaramoorthy P, et al. Multimodal selenium nanoshell-capped Au@mSiO$_2$ nanoplatform for NIR-responsive chemo-photothermal therapy against metastatic breast cancer. *NPG Asia Mater*. 2018;10:197–216.
12. Sun M, Xu L, Ma W, et al. Hierarchical plasmonic nanorods and upconversion core-satellite nanoassemblies for multimodal imaging-guided combination phototherapy. *Adv Mater*. 2016;28(5):898–904.
13. Taratula O, Schumann C, Duong T, Taylor KL, Taratula O. Dendrimer-encapsulated naphthalocyanine as a single agent-based theranostic nanoplatform for near-infrared fluorescence imaging and combinatorial anticancer phototherapy. *Nanoscale*. 2015;7(9): 3888–3902.
14. Deng R, Yi H, Fan F, et al. Facile exfoliation of MoS$_2$ nanosheets by protein as a photothermal-triggered drug delivery system for synergistic tumor therapy. *RSC Adv*. 2016;6(80):77083–77092.
15. Li W, Peng J, Tan L, et al. Mild photothermal therapy/photodynamic therapy/chemotherapy of breast cancer by Lyp-1 modified Docetaxel/IR820 Co-loaded micelles. *Biomaterials*. 2016;106:119–133.
16. Liu J, Liu K, Feng L, Liu Z, Xu L. Comparison of nanomedicine-based chemotherapy, photodynamic therapy and photothermal therapy using reduced graphene oxide for the model system. *Biomater Sci*. 2017;5(2):331–340.
17. Deng X, Chen Y, Cheng Z, et al. Rational design of a comprehensive cancer therapy platform using temperature-sensitive polymer grafted hollow gold nanospheres: simultaneous chemo/photothermal/photodynamic therapy triggered by a 650 nm laser with enhanced anti-tumor efficacy. *Nanoscale*. 2016;8(12):6837–6850.
18. Wo F, Xu R, Shao Y, et al. A multimodal system with synergistic effects of magneto-mechanical, photothermal, photodynamic and chemo therapies of cancer in graphene-quantum dot-coated hollow magnetic nanospheres. *Theranostics*. 2016;6(4):485–500.

19. Zhang M, Chen X, Zhang L, Li L, Su ZM, Wang C. Spadix-bract structured nanobowls for bimodal imaging-guided multidrug chemo-photothermal synergistic therapy. *Chemistry of Materials*. 2018;30(11):3722–3733.

20. Alves CG, Lima-Sousa R, de Melo-Diogo D, Louro RO, Correia IJ. IR780 based nanomaterials for cancer imaging and photothermal, photodynamic and combinatorial therapies. *Int J Pharm*. 2018;542(1–2):164–175.

21. Thawani JP, Amirshaghaghi A, Yan L, Stein JM, Liu J, Tsourkas A. Photoacoustic-guided surgery with indocyanine green-coated superparamagnetic iron oxide nanoparticle clusters. *Small*. 2017;13(37):1701300.

22. Chen J, Li X, Liu X, et al. Hybrid MoSe$_2$-indocyanine green nanosheets as a highly efficient phototheranostic agent for photoacoustic imaging guided photothermal cancer therapy. *Biomater Sci*. 2018;6(6):1503–1516.

23. You Q, Sun Q, Wang J, et al. A single-light triggered and dual-imaging guided multifunctional platform for combined photothermal and photodynamic therapy based on TD-controlled and ICG-loaded CuS@mSiO$_2$. *Nanoscale*. 2017;9(11):3784–3796.

24. Liu B, Li C, Xing B, Yang P, Lin J. Multifunctional UCNPs@PDA-ICG nanocomposites for upconversion imaging and combined photothermal/photodynamic therapy with enhanced antitumor efficacy. *J Mater Chem B*. 2016;4(28):4884–4894.

25. Liu C, Chen J, Zhu Y. Highly sensitive MoS2–Indocyanine green hybrid for photoacoustic imaging of orthotopic brain glioma at deep site. *Nanomicro Lett*. 2018;10(3):1–12.

26. Beziere N, Lozano N, Nunes A, et al. Dynamic imaging of PEGylated indocyanine green (ICG) liposomes within the tumor microenvironment using multi-spectral optoacoustic tomography (MSOT). *Biomaterials*. 2015;37(37c):415–424.

27. Li X, Schumann C, Albarqi HA, et al. A Tumor-activatable theranostic nanomedicine platform for NIR fluorescence-guided surgery and combinatorial phototherapy. *Theranostics*. 2018;8(3):767–784.

28. Loo CS, Lam NS, Yu D, Su XZ, Lu F. Artemisinin and its derivatives in treating protozoan infections beyond malaria. *Pharmacol Res*. 2017;117:192–217.

29. Sun C, Cao Y, Zhu P, Zhou B. A mitochondria-targeting artemisinin derivative with sharply increased antitumor but depressed anti-yeast and anti-malaria activities. *Sci Rep*. 2017;7:45665.

30. Kumari K, Keshari S, Sengupta D, Sabat SC, Mishra SK. Transcriptome analysis of genes associated with breast cancer cell motility in response to Artemisinin treatment. *BMC Cancer*. 2017;17(1):858.

31. Bhaw-Luximon A, Jhurry D. Artemisinin and its derivatives in cancer therapy: status of progress, mechanism of action, and future perspectives. *Cancer Chemother Pharmacol*. 2017;79(3):451–466.

32. Shahbazfar AA, Zare P, Mohammadpour H, Tayefi-Nasrabadi H, Emami SJ. Combination therapy enhanced the antitumor activity of artemisinin-iron in lung cancer Calu-6 cells. *Eur J Oncol*. 2017;22(1):31–37.

33. Letchmanan K, Shen SC, Ng WK, Tan RBH. Application of transglycosylated stevia and hesperidin as drug carriers to enhance biopharmaceutical properties of poorly-soluble artemisinin. *Colloids Surf B Biointerfaces*. 2018;161(10):83–93.

34. Bian X, Wu P, Sha H, et al. Anti-EGFR-iRGD recombinant protein conjugated silk fibroin nanoparticles for enhanced tumor targeting and antitumor efficiency. *Onco Targets Ther*. 2016;9:3153–3162.

35. Komiya K, Nakamura T, Nakashima C, et al. SPARC is a possible predictive marker for albumin-bound paclitaxel in non-small-cell lung cancer. *Onco Targets Ther*. 2016;9:6663–6668.

36. Deng W, Qiu J, Wang S, et al. Development of biocompatible and VEGF-targeted paclitaxel nanodrugs on albumin and graphene oxide dual-carrier for photothermal-triggered drug delivery in vitro and in vivo. *Int J Nanomedicine*. 2018;13:439–453.

37. Xin Y, Liu T, Yang C. Development of PLGA-lipid nanoparticles with covalently conjugated indocyanine green as a versatile nanoplatform for tumor-targeted imaging and drug delivery. *Int J Nanomedicine*. 2016;11:5807–5821.

38. Demircioglu F, Hodivala-Dilke K. αvβ3 Integrin and tumour blood vessels-learning from the past to shape the future. *Curr Opin Cell Biol*. 2016;42:121–127.